IEEE Access
Multidisciplinary | Rapid Review | Open Access Journal

Date of publication xxxx 00, 0000, date of current version xxxx 00, 0000.

Digital Object Identifier 10.1109/ACCESS.2017.DOI

Analysis of a Flexible Dual-Channel Octagonal Coil System for UHF MRI

NICOLA CURRELI[†1], MATTEO BRUNO LODI[†2], (Graduate Student Member, IEEE), ANDREA MELIS[†2], CLAUDIO PUDDU[3], SERGIO CASU[2], ALESSANDRO FANTI[2,4], (Member, IEEE), NIKOLA DJURIC[5], ALESSANDRA RETICO[6], AND GIUSEPPE MAZZARELLA[2,4], (Senior Member, IEEE)

[1]Functional Nanosystems, Istituto Italiano di Tecnologia, 16163 Genova, Italy (e-mail: nicola.curreli@iit.it)
[2]Department of Electrical and Electronic Engineering, University of Cagliari, Cagliari, Italy (email: alessandro.fanti@unica.it)
[3]POLARIS, Department of Infection, Immunity and Cardiovascular Disease, University of Sheffield, Sheffield, United Kingdom
[4]INFN-CA, Complesso Universitario di Monserrato, Cagliari, Italy
[5]Faculty of Technical Sciences, University of Novi Sad (email: ndjuric@uns.ac.rs)
[6]INFN-PI, Edificio C, Largo Bruno Pontecorvo, 3, 56127 Pisa, Italy

Corresponding author: Alessandro Fanti (e-mail: alessandro.fanti@unica.it).

This work was partially funded by the Advanced Techniques and Data Mining in MRI (nextMR), granted by INFN (CSN5) 2015-2017.
[†]These authors contributed equally to this work.

ABSTRACT Nowadays, MRI is focused on using ultra-high static magnetic fields (> 7 T) to increase the signal-to-noise ratio. The use of high fields, on the other hand, requires novel technical solutions as well as more stringent design criteria for specific absorption rate levels, reducing radiative effect and coil resistance. In this paper, two flexible RF coils for 7 T human magnetic resonance, and 298 MHz ultra-high frequency operations were analyzed and characterized. Imaging of lower human limbs is regarded as a case study. The lumped element theory and subsequent numerical simulations were used to fine-tune the single-coil element and the dual-coil array design, respectively. Here, we demonstrate how the shape, size, configuration, and presence of the sample influence the coil performance. The penetration depth of the B_1-field and the specific absorption rate values have been determined numerically using two numerical surface phantoms: saline and a multilayer human tissue. A preliminary study in the presence of a saline solution phantom has been carried out to develop and validate the dual-coil system. The frequency response of the dual-coil array was measured to assess its robustness when coupled to twelve human volunteers. We found that our design is robust to variations in the anatomical properties of the human thighs, and hence to coil bending. The presented approach can be useful for the implementation of flexible devices with high sensitivity levels and low specific absorption rate.

INDEX TERMS Coils, Optimization, Flexible printed circuits, Magnetic resonance imaging, Phantoms

I. INTRODUCTION

MAGNETIC resonance imaging (MRI) is a gold-standard technique for the assessment of several human diseases, and it is capable to offer a wide range of anatomical and functional information [1], [2]. MRI aims to provide clinically relevant images with high-contrast using the quantum principle of nuclear magnetic resonance [3]. Over the past 20 years, medical research has focused on the development of ultra-high-field (UHF – 7 T or higher) MRIs, thanks to their signal-to-noise ratio (SNR), which is almost double than that of a 4 T MRI [4]. They also allow acquiring high-resolution images in a short time [5]. One of the fundamental components of MRIs are the radiofrequency (RF) coils, which are responsible for transmitting and receiving signals from different areas of the human body and play a major role in determining the images' SNR [2]. RF coils can be mainly categorized into volume and surface coils [6]. The volume coils surround the tissue under exam (TUE) and have good RF homogeneity, which extends over a large area [6]. On the other hand, the surface coils are specifically designed for localized body regions and are placed in proximity of the region of interest (RoI). For this reason, the geometry of a surface coil is a very important feature in medical applications. Different circular, square, and decagonal surface coil configurations have been investigated, showing uniform field at low frequencies (<

127.74 MHz) [7]. Hexagonal coils have been proposed [8]–[10]. However, these shapes exhibited lower performance with stronger applied static magnetic fields, as the coil current path is electrically large, due to the limited wavelength ($\sim$ 1 m @ 300 MHz, in air), increasing the coil radiation losses [2], [11]. Therefore, the octagonal configuration has been proposed [12], allowing the current to flow more easily in UHF, avoiding high current densities at the corners of the coil, [12], [13], minimizing the lateral skin effect [14], achieving larger magnetic sensitivity [15], and providing improved SNR [13]. Moreover, the octagonal geometry benefits from a low manufacturing cost due to the ease of implementation, *e.g.*, through the screen-printing of the elements [16]. As a consequence, octagonal surface coils are receiving more and more attention, becoming the preferred choice over volume coils, despite the reduction of the field of view (FoV) [6]. Hence, increasing the FoV is one of the main goals to make the surface coils suitable for use in MRI: array coils allow covering a larger RoI than that obtained from a single surface coil, combining the local sensitivity of every single element [17], [18]. A variety of array coil designs have been proposed for UHF MRI, including microstrip elements [19], loop coils [20], dipole antennas [21], and dielectric resonant antennas [22]. Microstrip and multichannel transmit/receive (TX/RX) loop coils with independent phase and amplitude control, show a SNR on the RoI suitable for achieving specific absorption rate (SAR) levels within the IEC limits [23]. Similarly, dipole antenna arrays allow SAR levels of up to $\sim$ 60% compared to other techniques [24]. On the other hand, dielectric resonant antenna arrays, which use both resonant and non-resonant high permittivity structures, exhibit a sensitivity $\sim$ 25% higher than a loop gap resonator [25]. In the aforementioned designs, the elements of the array are decoupled using active strategies, which calls for metasurfaces design [20], [26] or electronics such as preamplifiers or decoupling circuits, *i.e.* complicated hardware solutions which implies a larger probe size, thus occupying a larger area [27], [28]. In addition, due to the materials and manufacturing techniques used, the probe costs inevitably increase [29]. For these reasons, using simple multiple loop coils as array elements is the most commonly used method for designing array coils [6]. Indeed, based on the investigated RoI, this design enables ease of implementation and allows choosing the optimal dimension and number of loops for the array. In this way, the array can be placed in close proximity to the RoI, allowing a higher SNR to be achieved even at larger depths (up to 60 mm), corresponding to better image quality [29], [30]. In this context, the realization of flexible coils is pivotal in view of the implementation of small size wearable RF arrays, offering several benefits [16], [31]. For example, a flexible receiver RF array can be tuned according to the subject (*e.g.*, considering intra-subject anthropometric variability), providing optimal conformal fitting by increasing the filling factor [32], [33], as well as improved comfort for the patient during the MRI exams [32]. At the same time, flexible coils

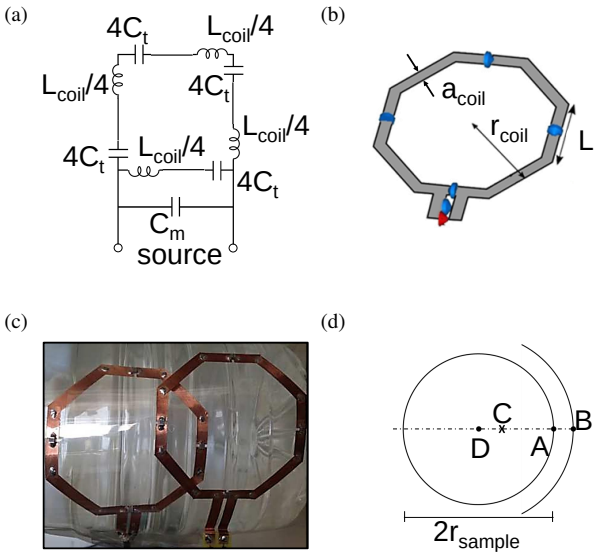

FIGURE 1: (a) Equivalent circuit of the RF flexible coil. (b) Single coil model, with the tuning and matching capacitors (blue dots). (c) Realized dual-coil array on a saline phantom solution or a simplified model of the human thigh. (d) Relative geometry of sample and sensor: C is the center of curvature of the sensor substrate.

result in a high FoV and a significant increase in SNR levels since the design is less sensitive to both dielectric and conductive properties of the subject [34]. However, in UHF, the anatomical features of the subjects could lead to alterations in the electromagnetic response of the flexible probes. In fact, the generated B_1-field and the coil impedance become simultaneously a complex function of the size, shape, and material of the coil, as well as the interaction of the coil with the patient, affecting its robustness and its frequency response [35], [36]. Furthermore, at 7 T, the size of the biological TUE becomes comparable, or even greater, to the working wavelength, so the interaction between biological tissues and the electromagnetic field becomes much stronger [37]. Therefore, it is of great importance to avoid inhomogeneity in the spatial distribution of the transmitted RF fields which could lead to high induced currents and produce large phase-shifted contributions to the B_1-field, with consequent critical problems in patient safety [2], [38]–[40].

In this work, the in-depth analysis of a two-channel octagonal geometry flexible matrix coil for 7 T MRI is presented. In order to perform the analysis, we have implemented and characterized a proof-of-concept array configuration. Our analysis shows that this design allows for robust and effective performance on a wide range of subjects, ensuring a complete and passive geometric decoupling without the use of preamplifiers, resulting in a smaller probe size, and therefore, a closer fit to the sample during the exam.

II. COIL AND ARRAY DESIGN

A simple but effective design methodology is presented for the case study of a two-channel array for imaging human thighs and femoral regions. The early-stage analysis and design of the UHF single RF coil, for the 7 T MRI dual-coil array, has been performed by using the LC circuit theory, treating the coils as a combination of inductive (L_{coil}), and capacitive (C_{coil}) lumped elements [41]. The lumped element circuit model is shown in Fig. 1a. As shown in Fig. 1b and Fig. 1c, two octagonal coils [24] with a thickness a_{coil} = 0.6 cm, side L = 3.44 cm and a radius r_{coil} = 4.5 cm have been considered. In order to match the coil to the 50 Ω impedance of the RF source (and of the input stage of the receiver), at the resonant frequency of f_r = 298 MHz, a tuning capacitance and a matching section are required [41]. C_{coil} can be estimated from the resonance condition of the equivalent LC circuit [42]:

$$C_{coil} = \frac{1}{\omega_0^2 L_{coil}} \tag{1}$$

where $\omega_0 = 2\pi f_r$ is the resonant angular frequency, while L_{coil} can be calculated according to the octagonal loop formula (Supplementary material) [12]. However, at UHF the coil electrical length is not small enough for the lumped-constant description to be accurate [2], hence Eq. 1 loses its accuracy, and also the current distribution could not be constant [2]. In addition, the search in the solution space is complicated by the possible influence of the bending of the flexible coil on the frequency response of the loaded array [2]. In order to get a constant current distribution along with the coil, we propose to divide the coil into N = 4 equal sections, each one shorter than λ/10 at ω_0 [43], and a connecting tuning capacitor (C_t) between each consecutive pair of sections given by:

$$C_t = N \cdot C_{coil} \tag{2}$$

In this way, the current in each section is constant and, because of the capacitors, is the same in each section. The value of C_t given by Eq. 2 can be assumed as a starting point for a pre-tuning procedure. In order to match the coil, a matching capacitance (C_m) is connected in parallel to the coil circuit as shown in Fig. 1a. Unlike C_t, the value of matching capacitors is an unknown function of the coil input impedance, *i.e.*, the load properties, which depends on the electromagnetic characteristic (namely, permittivity and conductivity) and the size and shape of the TUE [26]. Therefore, we performed tuning and matching optimization analysis using full-wave simulations via CST software to find suitable working conditions for MRI coil and array [44]. The values of C_t and C_m have been optimized by imposing f_r and input matching conditions (S_{11} < -15 dB at f_r) by performing extensive numerical experiments given a set of coil radii and arms lengths. [38]. Thus, it has been verified the strong mutual coupling between the coils and the TUE, carrying out the simulation in presence of the sample taken into account, *i.e.*, the saline solution phantom and the human thigh as shown in Fig. 1d. However, the proposed design approach could be adapted for other body areas. The two-channel array was used to image a larger RoI, with respect to a single loop coil. The array consists of two identical octagonal coils with a space between the two elements of $W = 0.75 \cdot r_{coil}$, which agrees with the theory of Roemer et al. [45], and to similar octagonal arrays operating at lower frequencies [46]. In this way, the strong influence on the input impedance is reduced [47], thus facilitating the implementation process and the robust performance against several types and shapes of loads. Indeed, by stabilizing the resistance, it is possible to retain almost constant quality factor (Q_{fact}) and sensitivity values. The curvature radius of the coil, defined in the geometrical reference frame shown in Fig. 1d, was not a free parameter in the CST (Microwave Studio, Simulia, 3DS, GE) simulations. In fact, for every given curvature, the values of C_t and C_m must be re-optimized, *i.e.*, the described design procedure should be carried out for different body regions. However, given the pre-design with the lumped theory and the fast numerical tuning and matching, the proposed methodology could be easily scaled and re-adapted for different cases, thus being of interest to other researchers in the field of UHF MRI [2], [26].

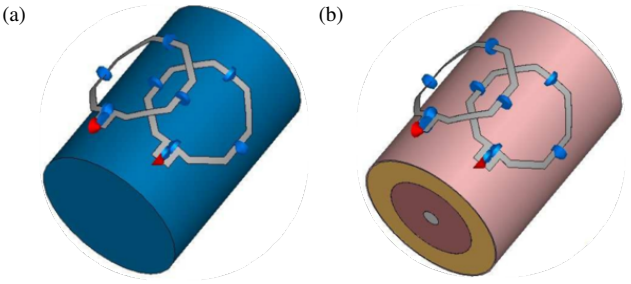

FIGURE 2: (a) Homogeneous saline phantom (sample S1). (b) Three layered numerical phantom: muscle, fat, bone tissues (sample S2).

III. ARRAY CHARACTERIZATION AND ANALYSIS

Since the resonant condition and the input match depend on the given sample materials, as well as on the curvature of the sample, the proposed dual-coil array was studied considering two different surface phantoms, represented in Fig. 2, as usally done in the literature. In the first model (Fig. 2a), a homogeneous cylinder (sample S1), with r_{sample} = 6 cm and l_{sample} = 16.8 cm, filled with a 0.1 M saline solution ($\varepsilon_r = 79 - j41.62$). This case study was considered the benchmark for the experimental validations of the realized dual-coil array for 7 T MRI. The second model (Fig. 2b) consists of a surface layered phantom that mimics the essential geometric and electromagnetic features of a human thigh, built as a multilayer cylinder (sample S2). A cylinder having the same dimensions as sample S1, with four layers (*i.e.*, bone, muscle, fat, skin), models the human thigh (see Tab. 1) [48]. The performance of the designed

Material	Thickness (cm)	Conductivity σ (S m^{-1})	Permettivity ε_r	Density (kg m^{-3})
Fat	2.2	0.0764	11.75	911
Muscle	3	0.7700	58.23	1090
Skin	0.1	0.6404	49.92	1190
Cortical bone	0.7	0.0824	13.45	1908

TABLE 1: Physical Properties of Tissues at 298 MHz [48].

dual-coil array for 7 T MRI together with the models was numerically analyzed with the purpose of testing the quality of field homogeneity and evaluating the SAR exposure of the proposed dual-coil array.

A. IN SILICO TEST WITH BIOLOGICAL SURFACE PHANTOM

From the periphery to the center, the phantom is composed of skin, fat, muscle, and bone [48]–[50], as shown in Fig. 2b. The physical parameters of the four human tissues used in the S2 samples are reported in Tab. 1 for the sake of completeness [48]. The designed dual-coil array for UHF MRI at 7 T was numerically tested with respect to the different geometry of the TUE and considering the influence of the curvature radius. The S2 sample was used to assess the coil sensitivity as a function of the phantom depth, according to [51], [52]. Furthermore, the SAR distribution and levels in the phantom were analyzed as follows [38]:

$$\mathrm{SAR} = \int_V \frac{\sigma |\mathbf{E}|^2}{\rho} \mathrm{dV} \tag{3}$$

where σ is the tissue conductivity, in S m^{-1}, ρ is the tissue density in, kg m^{-3}, and $\mathbf{E}$ is the induced electric field vector, in V m^{-1}, in the volume V. The SAR is volume-averaged according to IEEE/IEC 62704-1 regulation [53].

B. REALIZATION AND EXPERIMENTAL ASSESSMENT

In order to confirm the results obtained through the simulations, a plastic phantom (sample S3) having the same dimensions of the sample S1 containing the saline solution was used. The designed dual-coil array for UHF MRI has been realized using conductive copper tape (metal thickness of 400 μm on a thin flexible substrate (thickness of 0.2 mm, ε_r = 3.4, μ_r = 1), and the final double coil is shown in Fig. 1c.

The experimental measurements of the performances of the realized dual-coil array have been performed using a Hewlett Packard, 8720C Vector Network Analyzer [54]. The instrument was calibrated using the Open-Short-Load (OSL) method. Furthermore, experimental measurements were carried out on 12 human volunteers. The complex-valued scattering parameters (S_{11}) of the coil array was investigated on human thighs in order to demonstrate the robustness of the proposed design. The anthropometric characteristics of the subjects are reported in Table 2. This study was performed following the principles outlined in the Helsinki Declaration of 1975, as revised in 2000. Subjects were informed about the aim of the study, and they provided their informed consent.

Subj. ID.	Diameter (cm)	Length (cm)	Weight (kg)	Height (m)
SO1	17.2	46	70	1.76
SO2	16.8	48	80	1.75
SO3	19.4	45	72	1.74
SO4	19.0	47	72	1.67
SO5	16.8	43	76	1.73
SO6	16.2	45	70	1.69
SO7	16.2	41	77	1.76
SO8	19.7	42	85	1.80
SO9	18.4	42	72	1.74
SO10	14.9	42	74	1.70
SO11	14.3	48	71	1.66
SO12	16.4	41	70	1.78
Avg. $\pm$ std.	17.3 $\pm$ 1.8	44.1 $\pm$ 2.4	71.8 $\pm$ 5.4	1.73 $\pm$ 0.6

TABLE 2: Anthropometric Characteristics of the Volunteers.

IV. RESULTS

A. TEST ON SALINE SOLUTION

The dual-coil array for 7 T UHF MRI was firstly designed to resonate at 298 MHz and to be matched in presence of a saline solution phantom, having a radius of 6 cm (sample S1 in Fig. 2a). The guessing values for C_t are first derived from Eq. 2. Subsequently, the optimized C_t and C_m have been obtained through numerical simulations, as explained in Sect. II.B, and were found to be C_t = 5.4 pF and C_m = 1.5 pF, for each coil. These values are in accordance with devices having similar coil dimensions, and working frequency [20], [31], [55]. We found that the optimal spacing between the coils, required to passively decouple the array element, was found to be w = 6.75 cm, *i.e.* $0.75 \cdot r_{coil}$, for the geometry reported in Fig. 1b, confirming the results obtained by numerical simulations (Sect. II). The experimental measurements were then performed with the realized dual coil array on the sample S3, and the results were compared to the simulations. The simulated and experimental frequency responses of the $|S_{11}|$ have been found in good agreement with simulation results (*i.e.*, a maximum of 5 MHz shift and -3 dB difference), as shown in Fig. 3a. In order to understand and investigate how the TUE geometry affected the design and performance of the UHF array, the two-channel array was re-designed for three different values of curvature radii namely |BC| = 6, 8, 10 cm (at a distance r_{sample} = |AD| = 6 cm), considering a 0.1 M saline solution sample S1, as shown in Fig. 1c. The results found from the numerical design procedure are reported in Table 3. The corresponding S_{11} *vs.* frequency curves are shown in Fig. 3b. From the simulation results reported in Tab. 3 and in Fig. 3b it can be observed that as the radius of curvature increases (*i.e.*, as the sensor becomes flatter), the effect on the frequency shift is marginal, suggesting a negligible effect of the capacitive coupling with the load. Indeed, the value of C_t is almost constant, with a maximum variation of about 3%. This result suggests that a correct

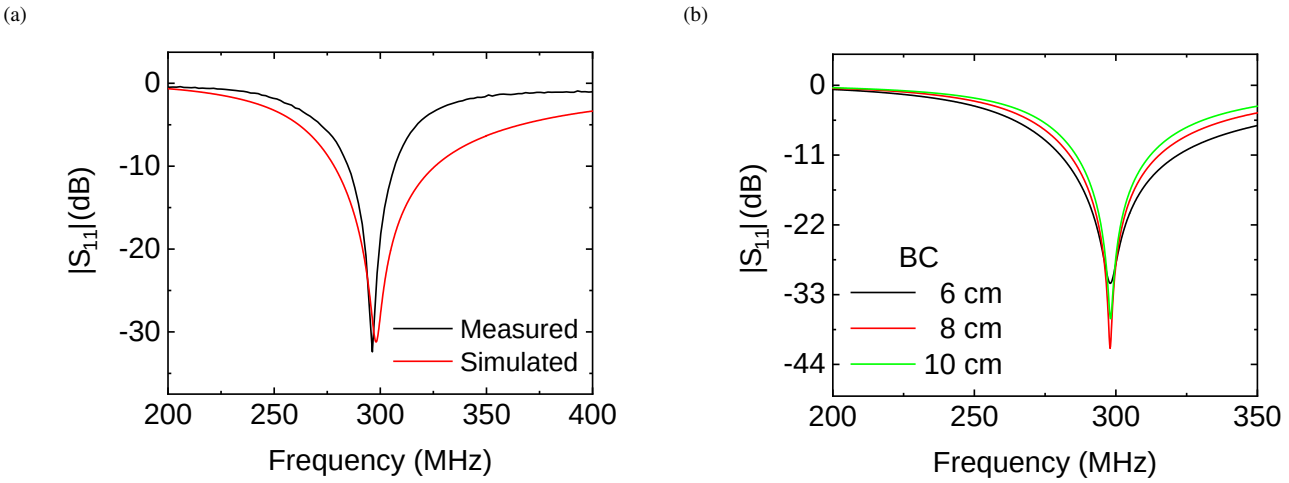

FIGURE 3: (a) Comparison between simulated and measured magnitude of S_{11} of the dual-coil array in presence of the saline phantom S3 (|BC| = 6). (b) Simulated reflection coefficient at the input of both coils of the dual coil sensor for the different curvature radii and capacitance values, which are reported in Tab. 3.

Material	|BC| = 6 cm	|BC| = 8 cm	|BC| = 10 cm
C_t (pF)	5.4	5.6	5.6
C_m (pF)	1.5	3.25	4.4
f_r (MHz)	297.95	297.95	298.1
$\|S_{11}\|$ (dB)	-31.21	-41.466	-36.44
Z_{11} (Ω)	50.43 - j0.59	51.28 - j0.74	50.23 - j0.22

TABLE 3: Simulations Results.

selection of the coil capacitors ensures a robust design for different loads. The input resistance of the loop requires a slight variation of C_m by increasing the radius of curvature, given an almost constant real part of the input impedance (less than 1%), and a negligible change in the complex impedance (> 0.50 Ω on average). The simulations about the field penetration in the saline phantom have been reported in the Supplementary materials. The provided numerical calculations proved the robust behavior of the dual coil array. For this reason, we selected a set of capacitance values capable of effectively match and tune the coil for any |BC|. This solution lowers the complexity of implementation, thus not requiring adaptive tuning strategies. Having demonstrated that the validity of the tuning and matching procedure, the numerical investigation focused on demonstrating that the conformal shape of the flexible array could improve the RF B_1-field sensitivity in the more complex and realistic case of the human-like phantom (sample S2) shown in Fig. 2b.

B. ANALYSIS AND PRELIMINARY CHARACTERIZATION FOR HUMAN MRI

The behavior and performances of the dual-coil array for UHF MRI at 7 T were investigated numerically by simulating the sensor loaded by the S2 sample. The array response was tested in silico by varying the thickness of fat and muscle layers for different curvature radii, considering the bone and skin layers size to be constant. The thickness variation of fat and muscle is known to strongly affect the coupling, field homogeneity, and SAR patterns [56], [57]. In order to investigate how the subject variability affects the UHF MRI exam, the maximum B_1^+ efficiency and the SAR inside the S2 sample were considered and reported in Fig. 4.

Fig. 4a–4c show a considerable asymmetry of the B_1^+ efficiency since at 7 T the wavelength is in the same range as the sample size. In fact, shorter wavelengths (and higher conductive currents) lead to greater phase changes [55]. Moreover, from Fig. S2, it is also possible to notice a discontinuity in the B_1^+-field, near the surface between muscle and fat. Indeed, a larger field intensity is observable, due to the higher conductivity of the muscle. Deeper, in the muscle the field efficiency is reduced due to the higher conductivity [58]. By observing the relationship B_1/E (Fig. S8 in Supplementary Materials), and on the basis of the SAR models of Fig. 4d–4f, it can be noticed that the coil efficiency decreases in the skin-muscle layer since the E-field is higher in this position. On the other hand, the coil's optimal matching is demonstrated on the phantom depth ($\sim$ 35 dB) and decreases as the bending increases. The volume-averaged SAR levels are shown in Fig. 4d–4f and the distribution is more inhomogeneous than the deposited power observed in the saline phantom case (Fig. S1, Supplementary material). For the human thigh phantom, given a curvature radius of |BC| = 6 cm, the computed maximum local SAR is lower than 4 W kg^{-1}, within the SAR limit of 10 W kg^{-1} [53]. Given the high sensitivity and the safe SAR levels, the robustness of the proposed UHF array was evaluated. The array was tuned and matched as previously described. The B_1^+-fields profiles in Fig. 5 and Fig. S4 (Supplementary materials) are in agreement with ref. [6], and at $\sim$ 3 cm and $\sim$ 4 cm of depth in the tissue phantom S2, independently by the radius of curvature. The simulation and experimental results for the

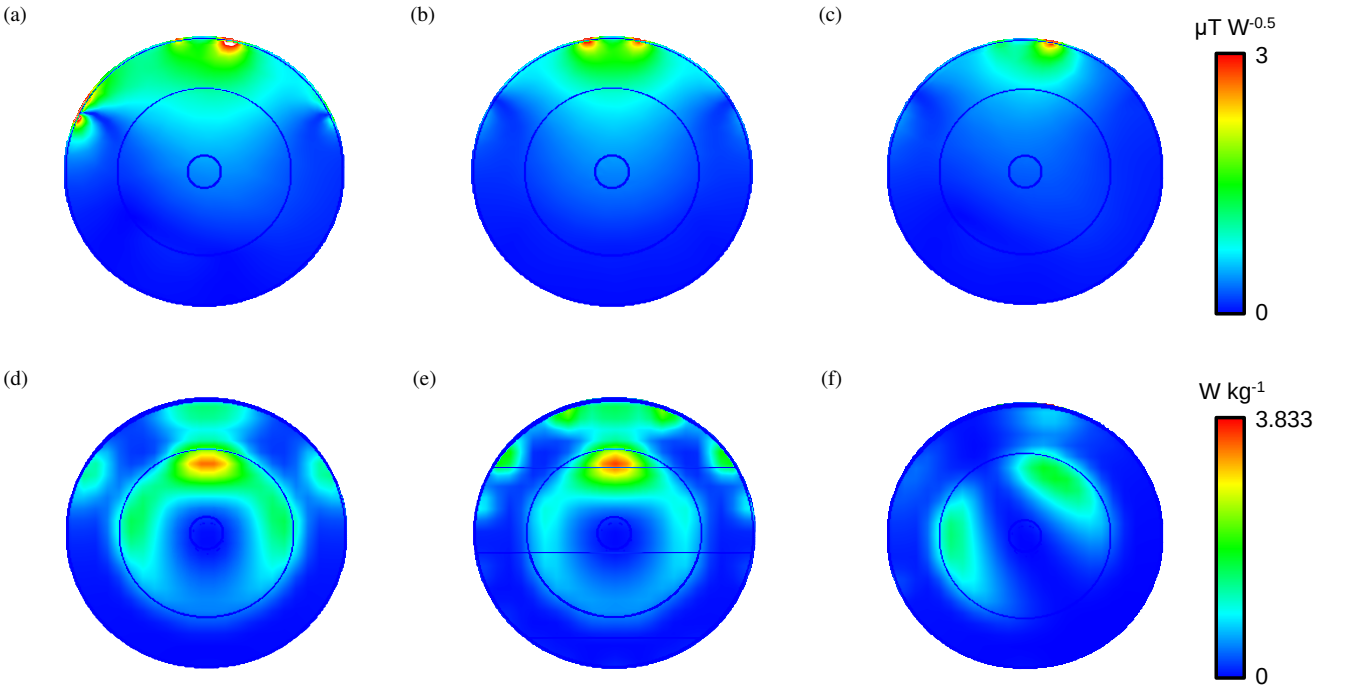

FIGURE 4: B_1^+ efficiency of the flexible dual-coil array with curvature of (a) 6 cm (b) 8 cm and (c) 10 cm over the body phantom S2. Specific Absorption Rate on the simulated body phantom S2 in W kg^{-1}, for different radius of curvature BC of the coil: (d) |BC| = 6 cm (e) |BC| = 8 cm and (f) |BC| = 10 cm.

S-parameters are shown in Fig. 6. From the simulations results, for a fixed radius of curvature (|BC| = 7 cm, C_t = 4.7 pF, C_m = 15 pF), the variation of muscle and fat tissues thickness for 2 cm and 3 cm has a negligible effect on the resonance frequency (a maximum difference of 5 MHz and a minimum of -2.5 MHz is found, as shown in Fig. S3 in Supplementary material), but affects the matching, as shown in Fig. 6. However, by comparing the in silico results with the experimental array $|S_{11}|$ in presence of the subjects, we found a variance of 2.5 MHz for f_r, at -15 dB while > 20 MHz from simulations. Therefore, both the array matching and tuning are not significantly affected by the anthropomorphic variability. The Q_{fact} of the coil was quantified for the loaded and unloaded coil from the S_{21} parameter *vs.* frequency. The relation between the loaded Q_{fact} and the unloaded Q_{fact} is an indicator of the coil sensitivity, and is reported as a measure to compare coil loops in their maximum efficiency to detect the MR signal [59]. For the unloaded coil a Q_{fact} of 96 is obtained (Fig. S5, Supplementary material). Thus, even the loaded quality factor ranges from 20 to a maximum of $\sim$ 35, for an average value of 24.577 (see Fig. S6, in Supplementary material). By comparing our findings to previous literature results (Supplementary material sec. 6), in [26] a four octagonal elements array, working at 298 MHz, showed a ratio of unloaded to loaded Q_{fact} varying from 3.2590 (34/11) to 1.204 (65/54), whilst, a similar array working at 64 and 127 MHz, presented values values in the range 6.7–11.4 when loaded (see Tab. S1). On the other hand, by considering the B_1^+-field efficiency, our flexible dual-coil system achieve a maximum value of $\sim$ 1 $\mu T/\sqrt{W}$, which is generally higher than the efficiencies (0.15-0.4 $\mu T/\sqrt{W}$) for other UHF MRI systems (supplementary material, Tab. S2) [60]–[63]. These results in the observed range of variation do not hamper the proposed design of the dual-coil array for UHF MRI at 7 T, in the case of human thighs confirming the robustness of the array.

V. CONCLUSION

In this work, we implement and fully characterize a flexible array of two octagonal coils for the imaging of the human thigh as a case study. The design methodology is based on passive decoupling of the elements and a numerical framework to achieve robust performances. Here, the proposed dual-coil UHF array for MRI was analyzed and validated both in silico and by using a saline solution. We carried out a numerical study on a multilayered human thigh phantom to evaluate the B_1-field distribution, homogeneity and SAR patterns. The influence of fat and muscle composition on the sensor response was also considered. The numerical simulations were validated by experimental measurements on human subjects. We found that the designed system has a constant B_1-field sensitivity at 3 – 4 cm of depth as |BC| increases. The sensitivity of our array is higher (> 0.5) deeper in the TUE *i.e.*, 5 mm *vs.* 3 cm [16]. The SAR levels lower as the array flattens, are always under the threshold values [53]. Moreover, we found better results than the traditional loop array, made of circular surface coil

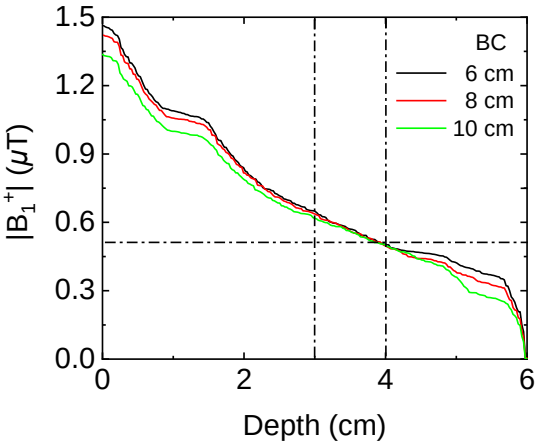

FIGURE 5: Average norm of the modulus of the B_1^+-field inside the numerical phantom S2 as a function of depth. In the plot the value of 0.5 μT is represented and the depth values of 3 and 4 cm from the phantom surface are highlighted for favoring the comprehension of the performances of the dual-coil array.

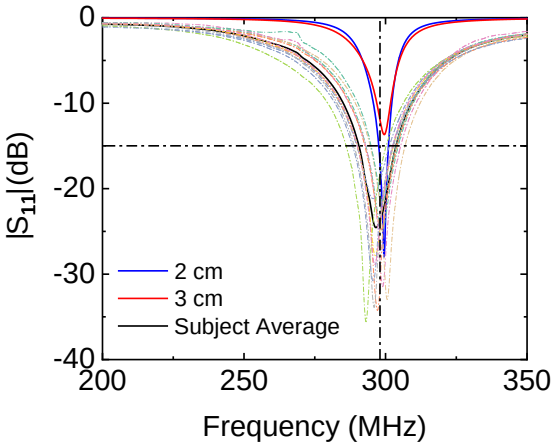

FIGURE 6: Magnitude of S_{11} parameter of an array coil over a S2 sample with muscle thickness of 2 cm (blue solid line) and 3 cm sample (red solid line), for a radius of curvature |BC| = 7 cm. The dashed lines represent the experimental measurements of the $|S_{11}|$ parameter for 12 subjects while the black curve is the average of the dashed lines.

working at 300 MHz, which demonstrated an asymmetric SAR distribution and a high peak value of 53.8 W kg^{-1} [64]. These promising results together with an unloaded to loaded Q_{fact} of 3.91, demonstrate the robustness of this design and allow us to forecast the use of the proposed dual-coil matrix for UHF for MRI at 7 T for different subjects. Given the numerical and experimental evidence, these findings could concern the study of the proposed conformal and flexible array on different body sites (*i.e.*, knee, wrist, neck) in order to benefit of its robust design. Future works will deal with the pre-clinical and in vivo tests for extracting magnetic resonance imaging with the proposed robust and flexible dual-coil array for UHF MRI.

REFERENCES

[1] B. Behzadnezhad, J. Andreae, S. A. Hurley, C. Filla, E. Mueller, B. D. Collick, N. Behdad, L. Populin, and A. B. McMillan, "Subject-specific, non-invasive helmet-restraint rf coil for awake, non-human primate mr imaging," *IEEE Journal of Electromagnetics, RF and Microwaves in Medicine and Biology*, vol. 3, no. 3, pp. 177–183, 2019.

[2] R. H. Caverly, "Rf aspects of high-field magnetic resonance imaging (hf-mri): Recent advances," *IEEE Journal of Electromagnetics, RF and Microwaves in Medicine and Biology*, vol. 3, no. 2, pp. 111–119, 2018.

[3] G. Liney, *MRI in clinical practice*. Springer Science & Business Media, 2007.

[4] J. T. Vaughan, M. Garwood, C. Collins, W. Liu, L. DelaBarre, G. Adriany, P. Andersen, H. Merkle, R. Goebel, M. Smith *et al.*, "7t vs. 4t: Rf power, homogeneity, and signal-to-noise comparison in head images," *Magnetic Resonance in Medicine: An Official Journal of the International Society for Magnetic Resonance in Medicine*, vol. 46, no. 1, pp. 24–30, 2001.

[5] C. Niu, Q. Wang, Y. Hu, Y. Wang, F. Tang, F. Liu, and S. Crozier, "Numerical design of high-efficiency whole-body gradient coils with a hybrid cylindrical-planar structure," *IEEE Transactions on Biomedical Engineering*, vol. 66, no. 6, pp. 1628–1636, 2018.

[6] J. T. Vaughan and J. R. Griffiths, *RF coils for MRI*. John Wiley & Sons, 2012.

[7] R. Rojas and A. O. Rodriguez, "Numerical study of the optimal geometry of mri surface coils," in *2007 29th Annual International Conference of the IEEE Engineering in Medicine and Biology Society*. IEEE, 2007, pp. 3890–3893.

[8] J. Lazovic, D. S. Stojkovic, C. M. Collins, Q. X. Yang, J. T. Vaughan, and M. B. Smith, "Hexagonal zero mode tem coil: A single-channel coil design for imaging multiple small animals," *Magnetic Resonance in Medicine: An Official Journal of the International Society for Magnetic Resonance in Medicine*, vol. 53, no. 5, pp. 1150–1157, 2005.

[9] M. K. Chaubey, M. Gupta, R. Harsh, and T. Bhuiya, "Multi-channel hexagonal surface coils for 1.5 t mri scanner," in *2016 International Conference on Communication Systems and Networks (ComNet)*. IEEE, 2016, pp. 236–240.

[10] N. Ugle, T. K. Bhuiya, R. Dapkar, D. Shinde, and S. Bagchi, "Design and comparison of rectangular, square and hexagonal rf coils for 1.5 t mri system," in *2018 9th International Conference on Computing, Communication and Networking Technologies (ICCCNT)*. IEEE, 2018, pp. 1–4.

[11] G. Barisano, F. Sepehrband, S. Ma, K. Jann, R. Cabeen, D. J. Wang, A. W. Toga, and M. Law, "Clinical 7 t mri: Are we there yet? a review about magnetic resonance imaging at ultra-high field," *The British journal of radiology*, vol. 92, no. 1094, p. 20180492, 2019.

[12] F. W. Grover, *Formulas and tables for the calculation of the inductance of coils of polygonal form*. US Government Printing Office, 1923, no. 468.

[13] J. R. Corea, P. B. Lechene, M. Lustig, and A. C. Arias, "Materials and methods for higher performance screen-printed flexible mri receive coils," *Magnetic resonance in medicine*, vol. 78, no. 2, pp. 775–783, 2017.

[14] G. Giovannetti, V. Hartwig, L. Landini, and M. F. Santarelli, "Classical and lateral skin effect contributions estimation in strip mr coils," *Concepts in Magnetic Resonance Part B: Magnetic Resonance Engineering*, vol. 41, no. 2, pp. 57–61, 2012.

[15] S. A. Winkler, J. Corea, B. Lechêne, K. OâBrien, J. R. Bonanni, A. Chaudhari, M. Alley, V. Taviani, T. Grafendorfer, F. Robb *et al.*, "Evaluation of a flexible 12-channel screen-printed pediatric mri coil," *Radiology*, vol. 291, no. 1, pp. 180–185, 2019.

[16] J. R. Corea, A. M. Flynn, B. Lechêne, G. Scott, G. D. Reed, P. J. Shin, M. Lustig, and A. C. Arias, "Screen-printed flexible mri receive coils," *Nature communications*, vol. 7, no. 1, pp. 1–7, 2016.

[17] J. Liu, J. Zheng, Q. Wang, W. Kainz, and J. Chen, "A transmission line model for the evaluation of mri rf-induced fields on active implantable medical devices," *IEEE Transactions on Microwave Theory and Techniques*, vol. 66, no. 9, pp. 4271–4281, 2018.

[18] M. B. Lodi, N. Curreli, A. Fanti, C. Cuccu, D. Pani, A. Sanginario, A. Spanu, P. M. Ros, M. Crepaldi, D. Demarchi *et al.*, "A periodic transmission line model for body channel communication," *IEEE Access*, vol. 8, pp. 160 099–160 115, 2020.

[19] B. Wu, C. Wang, D. A. Kelley, D. Xu, D. B. Vigneron, S. J. Nelson, and X. Zhang, "Shielded microstrip array for 7t human mr imaging," *IEEE transactions on medical imaging*, vol. 29, no. 1, pp. 179–184, 2009.

[20] X. Yan, J. C. Gore, and W. A. Grissom, "Self-decoupled radiofrequency coils for magnetic resonance imaging," *Nature communications*, vol. 9, no. 1, pp. 1–12, 2018.

[21] A. J. Raaijmakers, M. Italiaander, I. J. Voogt, P. R. Luijten, J. M. Hoogduin, D. W. Klomp, and C. A. van den Berg, "The fractionated dipole antenna: A new antenna for body imaging at 7 t esla," *Magnetic resonance in medicine*, vol. 75, no. 3, pp. 1366–1374, 2016.

[22] S. A. Aussenhofer and A. Webb, "High-permittivity solid ceramic resonators for high-field human mri," *NMR in Biomedicine*, vol. 26, no. 11, pp. 1555–1561, 2013.

[23] Y. Cho, A. Basir, and H. Yoo, "Adjustable rf transmitter head coil: Improving transmit efficiency with sar management for 7-t magnetic resonance imaging," *IEEE Transactions on Microwave Theory and Techniques*, vol. 69, no. 5, pp. 2686–2696, 2021.

[24] X. Zhang, K. Ugurbil, and W. Chen, "Microstrip rf surface coil design for extremely high-field mri and spectroscopy," *Magnetic Resonance in Medicine: An Official Journal of the International Society for Magnetic Resonance in Medicine*, vol. 46, no. 3, pp. 443–450, 2001.

[25] T. P. O'Reilly, T. Ruytenberg, and A. G. Webb, "Modular transmit/receive arrays using very-high permittivity dielectric resonator antennas," *Magnetic resonance in medicine*, vol. 79, no. 3, pp. 1781–1788, 2018.

[26] I. A. Elabyad, M. Terekhov, M. R. Stefanescu, D. Lohr, M. Fischer, and L. M. Schreiber, "Design and evaluation of a novel symmetric multichannel transmit/receive coil array for cardiac mri in pigs at 7 t," *IEEE Transactions on Microwave Theory and Techniques*, vol. 67, no. 9, pp. 3928–3945, 2019.

[27] C. Stumpf, M. Malzacher, and L.-P. Schmidt, "Radio frequency modeling of receive coil arrays for magnetic resonance imaging," *Journal of Imaging*, vol. 4, no. 5, p. 67, 2018.

[28] J. A. Nordmeyer-Massner, N. De Zanche, and K. P. Pruessmann, "Noise figure characterization of preamplifiers at nmr frequencies," *Journal of Magnetic Resonance*, vol. 210, no. 1, pp. 7–15, 2011.

[29] M. Kozlov and R. Turner, "Comprehensive analysis of transmit performance for an 8-element loop mri rf coil at 300 mhz," in *The 40th European Microwave Conference*. IEEE, 2010, pp. 328–331.

[30] A. M. Maunder, M. Daneshmand, P. Mousavi, B. Fallone, and N. De Zanche, "Comparison of high-density composite and surface coil arrays for mri of spherical imaging volumes," in *2014 IEEE MTT-S International Microwave Symposium (IMS2014)*. IEEE, 2014, pp. 1–4.

[31] S.-M. Sohn, L. DelaBarre, A. Gopinath, and J. T. Vaughan, "Rf head coil design with improved rf magnetic near-fields uniformity for magnetic resonance imaging (mri) systems," *IEEE transactions on microwave theory and techniques*, vol. 62, no. 8, pp. 1784–1789, 2014.

[32] J. D. Sánchez-Heredia, D. H. Johansen, R. B. Hansen, E. S. S. Hansen, C. Laustsen, V. Zhurbenko, and J. H. Ardenkjær-Larsen, "Improved decoupling for low frequency mri arrays using non-conventional preamplifier impedance," *IEEE Transactions on Biomedical Engineering*, vol. 66, no. 7, pp. 1940–1948, 2018.

[33] I. A. Elabyad, T. Herrmann, C. Bruns, J. Bernarding, and D. Erni, "Rf shimming and improved sar safety for mri at 7 t with combined eight-element stepped impedance resonators and traveling-wave antenna," *IEEE Transactions on Microwave Theory and Techniques*, vol. 66, no. 1, pp. 540–555, 2017.

[34] A. Mehmann, M. Varga, C. Vogt, A. Port, J. Reber, J. Marjanovic, K. P. Pruessmann, and G. Tröster, "On the bending and stretching of liquid metal receive coils for magnetic resonance imaging," *IEEE Transactions on Biomedical Engineering*, vol. 66, no. 6, pp. 1542–1548, 2018.

[35] E. Neufeld, M.-C. Gosselin, M. Murbach, A. Christ, E. Cabot, and N. Kuster, "Analysis of the local worst-case sar exposure caused by an mri multi-transmit body coil in anatomical models of the human body," *Physics in Medicine & Biology*, vol. 56, no. 15, p. 4649, 2011.

[36] C. Puddu, A. Fanti, N. Curreli, and G. Mazzarella, "Challenging the lumped birdcage coil model for high-field mri," in *2014 Loughborough Antennas and Propagation Conference (LAPC)*. IEEE, 2014, pp. 308–311.

[37] M. E. Ladd, P. Bachert, M. Meyerspeer, E. Moser, A. M. Nagel, D. G. Norris, S. Schmitter, O. Speck, S. Straub, and M. Zaiss, "Pros and cons of ultra-high-field mri/mrs for human application," *Progress in nuclear magnetic resonance spectroscopy*, vol. 109, pp. 1–50, 2018.

[38] K. N. Bocan, M. H. Mickle, and E. Sejdić, "Simulating, modeling, and sensing variable tissues for wireless implantable medical devices," *IEEE Transactions on Microwave Theory and Techniques*, vol. 66, no. 7, pp. 3547–3556, 2018.

[39] Z. Wang, J. Zheng, Y. Wang, W. Kainz, and J. Chen, "On the model validation of active implantable medical device for mri safety assessment," *IEEE Transactions on Microwave Theory and Techniques*, vol. 68, no. 6, pp. 2234–2242, 2019.

[40] A. Melis, S. Casu, A. Fanti, G. Mazzarella, C. Puddu, and P. Boccacci, "Robustness of flexible 7t-mri coil behaviour," in *2017 International Applied Computational Electromagnetics Society Symposium-Italy (ACES)*. IEEE, 2017, pp. 1–2.

[41] J. Mispelter, M. Lupu, and A. Briguet, *NMR probeheads for biophysical and biomedical experiments: theoretical principles and practical guidelines*. World Scientific Publishing Company, 2015.

[42] D. Hoult, "The nmr receiver: a description and analysis of design," *Progress in Nuclear Magnetic Resonance Spectroscopy*, vol. 12, no. 1, pp. 41–77, 1978.

[43] J. Jin, *Electromagnetic analysis and design in magnetic resonance imaging*. CRC press, 1998, vol. 1.

[44] A. Kordzadeh and N. De Zanche, "Control of mutual coupling in high-field mri transmit arrays in the presence of high-permittivity liners," *IEEE Transactions on Microwave Theory and Techniques*, vol. 65, no. 9, pp. 3485–3491, 2017.

[45] P. B. Roemer, W. A. Edelstein, C. E. Hayes, S. P. Souza, and O. M. Mueller, "The nmr phased array," *Magnetic resonance in medicine*, vol. 16, no. 2, pp. 192–225, 1990.

[46] R. G. Henry, N. J. Fischbein, W. P. Dillon, D. B. Vigneron, and S. J. Nelson, "High-sensitivity coil array for head and neck imaging," *American journal of neuroradiology*, vol. 22, no. 10, pp. 1881–1886, 2001.

[47] M. A. Ohliger and D. K. Sodickson, "An introduction to coil array design for parallel mri," *NMR in Biomedicine: An International Journal Devoted to the Development and Application of Magnetic Resonance In vivo*, vol. 19, no. 3, pp. 300–315, 2006.

[48] M. J. Ackerman, "The visible human project," *Proceedings of the IEEE*, vol. 86, no. 3, pp. 504–511, 1998.

[49] D. Hoult, C.-N. Chen, and V. Sank, "Quadrature detection in the laboratory frame," *Magnetic Resonance in Medicine*, vol. 1, no. 3, pp. 339–353, 1984.

[50] D. Krstić and D. Nikezić, "Input files with ornlâmathematical phantoms of the human body for mcnp-4b," *Computer Physics Communications*, vol. 176, no. 1, pp. 33–37, 2007.

[51] N. E. M. Association *et al.*, "Determination of image uniformity in diagnostic magnetic resonance images," *NEMA Standard Publications, MS 3*, 2005.

[52] A. Hassan, I. Elabyed, J. Mallow, T. Herrmann, J. Bernarding, and A. Omar, "Optimal geometry and capacitors distribution of 7t mri surface coils," in *The 40th European Microwave Conference*. IEEE, 2010, pp. 1437–1440.

[53] I. E. Commission *et al.*, "Medical electrical equipment-part 2-33: Particular requirements for the basic safety and essential performance of magnetic resonance equipment for medical diagnosis," *IEC 60601-2-33 Ed. 3.0*, 2010.

[54] Keysight, "8720C Microwave Network Analyzer Keysight (formerly Agilent's Electronic Measurement)." [Online]. Available: https://www.keysight.com/en/pd-1000002254{\%}3Aepsg{\%}3Apro-pn-8720C/microwave-network-analyzer?cc=IT{\&}lc=ita.

[55] C. M. Collins, S. Li, and M. B. Smith, "Sar and b1 field distributions in a heterogeneous human head model within a birdcage coil," *Magnetic Resonance in Medicine*, vol. 40, no. 6, pp. 847–856, 1998.

[56] G. Muntoni, A. Fanti, G. Montisci, and M. Muntoni, "A blood perfusion model of a rms tumor in a local hyperthermia multi-physic scenario: A preliminary study," *IEEE Journal of Electromagnetics, RF and Microwaves in Medicine and Biology*, vol. 3, no. 1, pp. 71–78, 2018.

[57] M. B. B. Lodi, G. Muntoni, A. Ruggeri, A. Fanti, G. Montisci, and G. Mazzarella, "Towards the robust and effective design of hyperthermic devices: Case study of abdominal rhabdomyosarcoma with 3d perfusion," *IEEE Journal of Electromagnetics, RF and Microwaves in Medicine and Biology*, 2020.

[58] M. V. Vaidya, C. M. Collins, D. K. Sodickson, R. Brown, G. C. Wiggins, and R. Lattanzi, "Dependence of and field patterns of surface coils on the electrical properties of the sample and the mr operating frequency," *Concepts in Magnetic Resonance Part B: Magnetic Resonance Engineering*, vol. 46, no. 1, pp. 25–40, 2016.

[59] B. Gruber, M. Froeling, T. Leiner, and D. W. Klomp, "Rf coils: A practical guide for nonphysicists," *Journal of magnetic resonance imaging*, vol. 48, no. 3, pp. 590–604, 2018.

[60] A. Andreychenko, H. Kroeze, D. W. Klomp, J. J. Lagendijk, P. R. Luijten, and C. A. van den Berg, "Coaxial waveguide for travelling wave mri at

ultrahigh fields," *Magnetic Resonance in Medicine*, vol. 70, no. 3, pp. 875–884, 2013.

[61] B. Zhang, D. K. Sodickson, R. Lattanzi, Q. Duan, B. Stoeckel, and G. C. Wiggins, "Whole body traveling wave magnetic resonance imaging at high field strength: homogeneity, efficiency, and energy deposition as compared with traditional excitation mechanisms," *Magnetic resonance in medicine*, vol. 67, no. 4, pp. 1183–1193, 2012.

[62] C. Snyder, L. Delabarre, S. Moeller, J. Tian, C. Akgun, P.-F. Van de Moortele, P. Bolan, K. Ugurbil, J. Vaughan, and G. Metzger, "Comparison between eight-and sixteen-channel tem transceive arrays for body imaging at 7 t," *Magnetic resonance in medicine*, vol. 67, no. 4, pp. 954–964, 2012.

[63] P. S. Athalye, M. M. Ilić, P.-F. van de Moortele, A. J. Kiruluta, and B. M. Notaroš, "Multi-channel helical-antenna inner-volume rf coils for ultra-high field mr scanners," *Concepts in Magnetic Resonance Part B: Magnetic Resonance Engineering*, vol. 48, no. 4, p. e21405, 2018.

[64] B. Zhang, D. K. Sodickson, and M. A. Cloos, "A high-impedance detector-array glove for magnetic resonance imaging of the hand," *Nature biomedical engineering*, vol. 2, no. 8, pp. 570–577, 2018.

NICOLA CURRELI after the M.Sc. degree from the University of Genoa (Genoa, Italy), in 2016, received the Ph.D. degree in Electronic Engineering, from the University of Cagliari (Cagliari, Italy) and the Italian Institute of Technology - IIT (Genoa, Italy), in 2020. In 2019 he was visiting researcher with the Physics and Mechanical Engineering Departments at Columbia University in the City of New York (New York, USA). After the Ph.D., he held a fellow position at Graphene Labs - IIT in the WP12 (Energy storage) of the Graphene Core 2 project - Graphene flagship. He is currently a post-doc at the Functional Nanosystems group - IIT. His research activity includes the study of low-dimensional materials, their characterization, and their application in the field of photonics, as well as the design, implementation, and analysis of linear and nonlinear integrated optical and microwave devices and antennas.

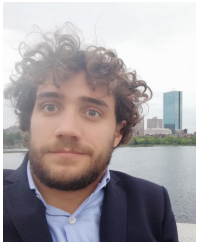

MATTEO BRUNO LODI (Graduate Student Member, IEEE) received the bachelor's degree in biomedical engineering from the University of Cagliari, Cagliari, in 2016, and the master's degree in biomedical engineering from Politecnico di Torino, Turin, Italy, in 2018. He received the Ph.D. degree in electronic engineering and computer science from the University of Cagliari in 2022. His research activity deals with the modeling of bioelectromagnetic phenomena, especially hyperthermia treatment; the study, manufacturing, and synthesis of magnetic biomaterials for tissue engineering applications; and the use of microwave for biotechnology and environmental applications. He was awarded as Young Scientists at General Assembly and Scientific Symposium of URSI 2020 and 2021. He has been appointed as Representative for the Young Professionals of IEEE Region 8 for the Nanotechnology Council. He is a member of the Editorial Board of the IEEE Future Directions Technology Policy and Ethics newsletter.

ANDREA MELIS received his Bachelor's degree in biomedical engineering in 2017 at University of Cagliari (Italy) where he worked as an assistant researcher. His research interests involve the EM modeling and developing of RF coils at low and high frequencies, the design and realization of WSN systems for the monitoring of industrial processes, such as bread manufacturing.

CLAUDIO PUDDU received his Bachelor degree in Biomedical Engineering in 2014 from the University of Cagliari (Italy), and he also worked as an assistant researcher from 2013 to 2014. In 2017 was a visiting student at National Institute of Nuclear Physics (INFN) in Pisa, Italy and in the same year obtained his Master degree, from University of Genova, Italy. He is currently a Ph.D. student at University of Sheffield, UK. His research interests are the EM modeling and developing of RF coils at low and high frequencies.

SERGIO CASU graduated in Electronic Engineering, received the M.Sc. degree in Telecommunication Engineering at the University of Cagliari in 2014. He obtained the Ph.D. degree in Electronic Engineering and Computer Science in 2018 with research activities in the field of electromagnetism involving the design and characterization of resonant cavities as biological reactor, design of RF coil for ultra-high field MRI, design of antennas for UHF RFID, design of antennas for biomedical applications, and use of microwaves for farmland disinfection.

ALESSANDO FANTI received the Laurea degree in electronic engineering and Ph.D. degree in Electronic Engineering and computer science from the University of Cagliari, Cagliari, Italy, in 2006 and 2012, respectively. He worked as post-doctoral fellow in the Electromagnetic Group at the University of Cagliari from 2013 to 2016, where he is currently an Assistant Professor. His research activity involves the use of numerical techniques for modes computation of guiding structures, optimization techniques, design and characterization of resonant cavities as biological reactor analysis and design of waveguide slot arrays, analysis and design of patch antennas, modelling of bio-electromagnetic phenomena, and radio propagation in urban environment.

ALESSANDRA RETICO Ph.D., is a researcher at INFN since 2005. Her main research interests are in medical imaging (RX, CT, MRI, PET-MR), image processing and analysis with standard and innovative techniques, including machine-learning and deep-learning based methods. She developed and validated on large samples automated systems for lung nodule detection on screening CT. She has been the coordinator of several INFN-funded research projects in this field (SEVEN, 2011-2012, and TESLA, 2013–2014), focused in technological development for Ultra-High-Field MRI, and the Pisa unit coordinator of the nextMR (Advanced Techniques and Data Mining in MRI) project (2015–2017), and currently the coordinator of the Artificial Intelligence in Medicine research project (2019–2021). She was research unit coordinator of the project "Supporting an early autism spectrum disorder diagnosis through the support vector machine approach" (funded by Italian Ministry of Health, GR-2010-2317873) and of the ARIANNA project ("Interdisciplinary research platform for neuroimaging analysis in Autism Spectrum Disorders", 2016–2018, funded by PAR-FAS 2007–2013), where an informatics platform has been developed to facilitate MRI data collection and thus neuroimaging-based research on Autism Spectrum Disorders (ASD). She is a member of the "Train the Brain" consortium and of the ENIGMA (Enhancing Neuro Imaging Genetics through Meta-Analysis)–ASD working group.

NIKOLA DJURIC (M'99) was born in Novi Sad, Serbia, in 1973. He received the M.Sc. and Ph.D. degrees in Telecommunication and Signal Processing from the Faculty of Technical Sciences (FTN-UNS), University of Novi Sad, in 2003 and 2009, respectively. From 1997 to 2010 he was a Teaching Assistant; from 2010 to 2015 Assistant Professor; while since 2015 he has been an Associate Professor at FTN-UNS , since 2000, as full professor. He is the author of more than 70 journal and conference articles. His research interests include computational and applied electromagnetics, with experience in environmental electromagnetic field (EMF) measurement and monitoring for EMF compliance testing, estimation, and simulation of EMF whole-body exposure.

GIUSEPPE MAZZARELLA (S '82, M '90, SM '99), graduated Summa with Laude in Electronic Engineering from the Università Federico II of Naples in 1984 and subsequently obtained the PhD in Electronic Engineering and Computer Science in 1989. In 1990 he became Assistant Professor at the Dipartimento di Ingegneria Elettronica at the Università Federico II of Naples. Since 1992 he is with the Dipartimento di Ingegneria Elettrica ed Elettronica of the Università di Cagliari, first as associate professor and then, since 2000, as full professor, teaching courses in Electromagnetics, Microwave, Antennas and Remote Sensing. His research activity has focused mainly on: efficient design of large arrays of slots, power synthesis of array factor, with emphasis on inclusion of constraints, microwave holography techniques for the diagnosis of large reflector antennas, use of evolutionary programming for the solution of inverse problems, in particular problems of synthesis of antennas and periodic structures. He is author (or coauthor) of over 70 papers in international journals, and is a reviewer for many EM journals.